ChemComm

COMMUNICATION

View Article Online
View Journal | View Issue

Cite this: *Chem. Commun.*, 2025, **61**, 8375

Received 11th March 2025,
Accepted 7th May 2025

DOI: 10.1039/d5cc01308a

rsc.li/chemcomm

Efficient direct regeneration of spent $LiFePO_4$ from various degradation states for sustainable battery recycling†

Jintao Zhang, [a] Song Lin Zhang,[a] Nguk Neng Tham,[a] Hui Ru Tan,[a] Wanwan Wang, [a] Yi Ren,[a] Qing Wang *[b] and Zhaolin Liu *[a]

Efficient regeneration of spent $LiFePO_4$ is essential for the sustainable management of end-of-life electric vehicle batteries, given their significant market share. A universal method capable of directly regenerating spent $LiFePO_4$ from cells with varying states of health is crucial for practical implementation. Herein, we developed an oxalic acid/lithium hydroxide-based regeneration approach that effectively restores mixed spent $LiFePO_4$, achieving a high specific capacity of 163.1 mA h g^{-1} at 0.1C.

With the rapid expansion of the EV market, the volume of retired EV batteries has grown significantly in recent years, a trend expected to accelerate globally in the coming decades.[1–3] Effective management of end-of-life (EoL) EV batteries is crucial not only for environmental sustainability but also for economic viability due to the high value and potential toxicity of battery materials.[2,4–6] Battery recycling represents the final stage of a battery's lifecycle, though repurposing or remanufacturing may precede it.[5,7] Recycling methods are generally classified based on their end products: if the process yields raw materials for lithium-ion battery (LIB) production, it is termed recovery;[8–12] if the end product is active materials suitable for direct reuse in LIBs, it is termed direct regeneration.[13–20]

Conventional recovery, primarily based on extracting key valuable materials (*e.g.*, Li, Co, Ni), has already been industrialized due to its operational simplicity.[11,12,21] This method is particularly advantageous for lithium cobalt oxide (LCO)[22,23] and nickel manganese cobalt (NMC) batteries.[10,24,25] However, recovering lithium iron phosphate (LFP) batteries is less economically attractive, as the only recoverable high-value products are lithium-based salts (*e.g.*, lithium hydroxide or lithium carbonate). While lithium salts have higher unit mass values than LFP (Fig. 1(a)), direct regeneration of 1 ton of spent LFP (denoted as S-LFP) batteries can double the product value (Fig. 1(b) and Table S1, ESI†), making this approach significantly more viable (Fig. S1, ESI†).

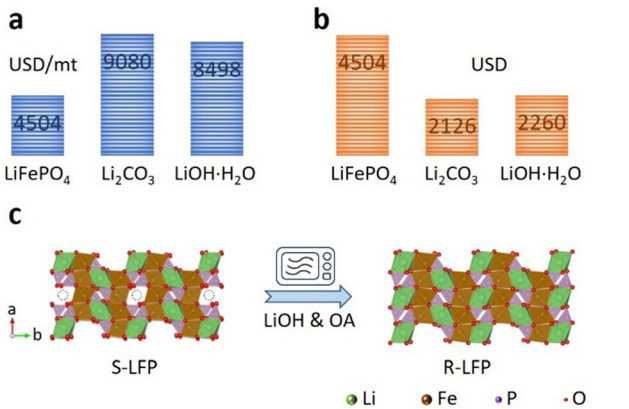

Fig. 1 (a) Market price of battery-grade $LiFePO_4$, Li_2CO_3, and $LiOH{\cdot}H_2O$ (unit: US dollars per metric ton) and (b) end-of-product price of recycling 1 ton of spent $LiFePO_4$ (assuming 100% conversion). (c) Illustration of recovery mechanism of S-LFP. (R-LFP denotes regenerated LFP).

Existing direct regeneration strategies for LFP batteries primarily focus on replenishing lithium deficiencies in spent LFP.[19,26] These methods typically utilize a reductant—often an organic acid, such as citric acid,[27] L-ascorbic acid,[18,28,29] or tartaric acid,[16,17] along with a lithium source, typically lithium hydroxide. While these methods have shown promise, their application remains largely confined to laboratory-scale studies, with several factors limiting their practical feasibility. One key challenge is whether a given method is suitable for mixed spent LFP derived from different battery sources. To address this issue, we developed a rapid microwave-assisted hydrothermal method (Table S2, ESI†) utilizing oxalic acid (OA) as a reducing and chelating agent, along with lithium hydroxide as the lithium source. This method was applied to mixed spent LFP from various batteries with different states of health (SOH). Additionally, we

[a] *Institute of Materials Research and Engineering (IMRE), Agency for Science, Technology and Research (A*STAR), 2 Fusionopolis Way, Innovis #08-03, Singapore 138634, Republic of Singapore. E-mail: zl-liu@imre.a-star.edu.sg*
[b] *Department of Materials Science and Engineering, National University of Singapore, Singapore 117576, Republic of Singapore. E-mail: msewq@nus.edu.sg*

† Electronic supplementary information (ESI) available. See DOI: https://doi.org/10.1039/d5cc01308a

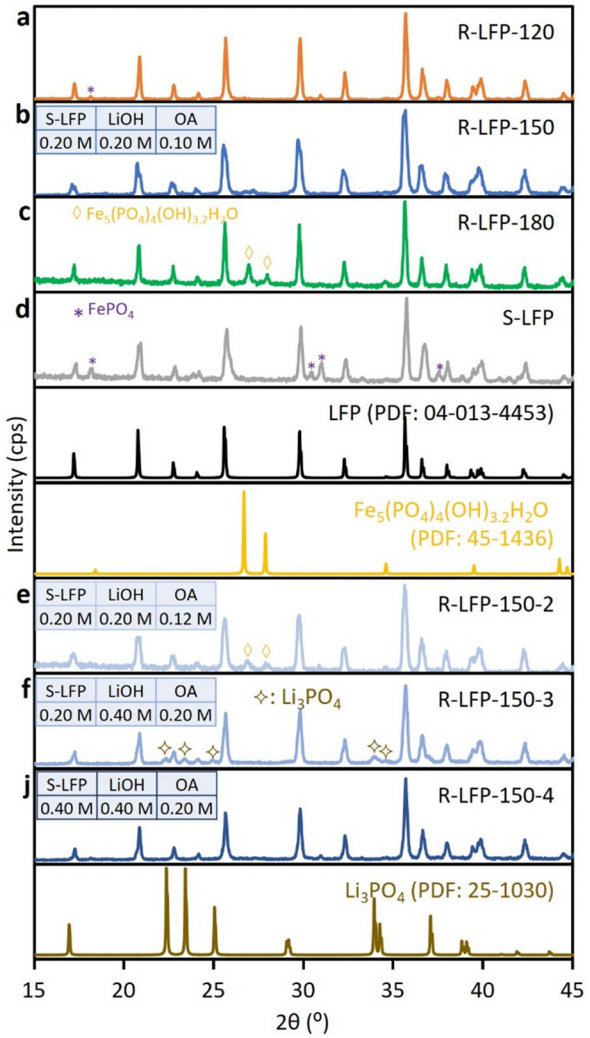

Fig. 2 XRD Patterns of R-LFP-120 (a), R-LFP-150 (b), R-LFP-180 (c), S-LFP (d), R-LFP-150-2 (e), R-LFP-150-3 (f) and R-LFP-150-4 (j). 120, 150, 180 indicate the reaction temperature (°C). R-LFP denotes regenerated LFP.

systematically investigated the effects of reaction temperature and the molar ratios of OA, lithium hydroxide (LiOH), and spent LFP on the regeneration efficiency.

We cycled 1.5 A h LFP cylindrical cells to different states of health (SOH), ranging from 55% to 70% (Fig. S2, ESI†). The spent LFP (S-LFP) was obtained from these cells and mixed together. The separation and purification processes are detailed in the ESI.† The XRD pattern of S-LFP (Fig. 2(d)) exhibits specific peaks similar to reported result,[27] with impurity peaks of $FePO_4$ appearing around 18 degrees.

We first examined the impact of reaction temperature on direct LFP regeneration. XRD analysis (Fig. 2(a)–(c)) revealed that excessively high temperatures (180 °C) led to the formation of $Fe_5(PO_4)_4(OH)_3{\cdot}2H_2O$ (PDF: 45-1436), an undesirable impurity. Meanwhile, $FePO_4$ residues persisted in R-LFP-120, likely due to the lower reaction rate at 120 °C. The optimal temperature was 150 °C, as R-LFP-150 exhibited the best match with simulated LFP (PDF: 04-013-4453).

Based on literature findings, organic acids play a critical role in the direct regeneration of spent LFP, acting as reducing agent.[16,18,27] To assess the impact of increasing OA concentration, we added 20 wt% more OA to the reactor while maintaining constant amounts of S-LFP and LiOH. The XRD pattern of R-LFP-150-2 (Fig. 2(e)) indicated that excessive OA resulted in the formation of the $Fe_5(PO_4)_4(OH)_3{\cdot}2H_2O$ phase, similar to that observed in R-LFP-180 (Fig. 2(c)). Overall, a LiOH/OA molar ratio of 2 : 1 was determined to be optimal for lithium replenishment in spent LFP at 150 °C.

Considering the LiOH/OA molar ratio of 2 : 1 as a regeneration agent (RA), the ratio of S-LFP to RA is critical for practical applications. Doubling the amount of RA compared to R-LFP-150 resulted in R-LFP-150-3, where the XRD pattern (Fig. 2(f)) showed the presence of Li_3PO_4 impurities. These findings suggest that excessive RA promotes the formation of the Li_3PO_4 phase. To further optimize the process, we doubled the concentration of all reactants, leading to R-LFP-150-4. The XRD pattern (Fig. 2(j)) displayed distinct LFP-specific peaks, indicating that adjusting feedstock concentrations while maintaining the correct molar ratios is a promising strategy to reduce wastewater production during LFP direct regeneration.

We investigated the chemical valence changes of regenerated LFP (denoted as R-LFP) using X-ray photoelectron spectroscopy (XPS) (Fig. 3(a)). The results indicate that S-LFP exhibited Fe^{3+} peaks at approximately 712.00 eV and Fe^{2+} peaks at around 710.19 eV in the Fe $2p_{3/2}$ region. After regeneration, R-LFP showed only Fe^{2+} peaks (710.35 eV), confirming that most Fe^{3+} was reduced during the hydrothermal process under the reductive influence of oxalic acid. The valence states of Fe were further verified by electron energy loss spectroscopy (EELS) (Fig. 4(b)). Changes in Fe valence states were evident from the energy loss shifts of the Fe L_2-edge and L_3-edge.[30] The lower shift of the Fe L_3-edge in R-LFP-150 compared to S-LFP indicates the successful reduction of Fe^{3+} to Fe^{2+} during regeneration.

The morphology of R-LFP-150 and S-LFP was examined using scanning electron microscopy (SEM) and high-resolution transmission electron microscopy (HRTEM). The SEM images of R-LFP-150 (Fig. 3(c) and Fig. S3a, b (ESI†)) revealed a particle size comparable to that of S-LFP (Fig. 3(d) and Fig. S3c, d (ESI†)). The HRTEM image of R-LFP-150 (Fig. 3(e)) displayed well-defined lattice fringes with an interplanar spacing of 0.42 nm, corresponding to the (101) crystal plane of LFP.[20] The elemental composition of R-LFP-150 and S-LFP was analyzed *via* energy-dispersive X-ray spectroscopy (EDX) (Fig. S4, ESI†). Both materials exhibited signals for C, O, Fe, and P, while no detectable signals of fluorine (F) or aluminum (Al) were observed in S-LFP. This indicates that the regeneration process was highly effective, ensuring the complete removal of Al fragments, binder, and electrolyte salt from S-LFP.

To evaluate the electrochemical performance and regeneration efficacy of our method, we assembled 2032-type coin cells using R-LFP-120, R-LFP-150, R-LFP-180, and S-LFP as electrodes. As shown in Fig. 4(a), the R-LFP-150 exhibited an initial capacity of 163.1 mA h g^{-1} at a 0.1C rate, which is significantly

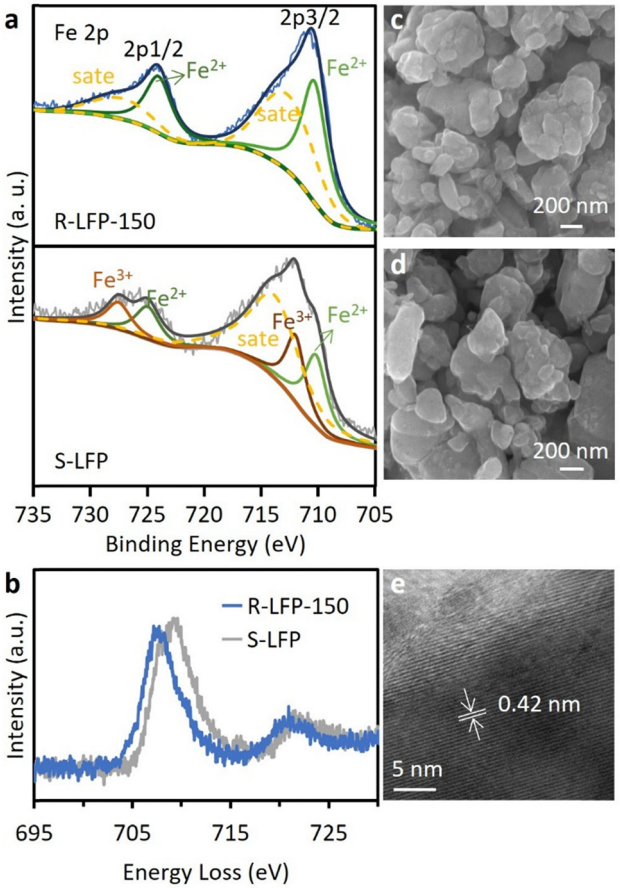

Fig. 3 (a) Fe 2p spectra of R-LFP-150 and S-LFP. (b) Fe L-edge ELLS spectra of a representative R-LFP-150 and S-LFP. FESEM images of (c) R-LFP-150 and (d) S-LFP. (e) HRTEM of R-LFP-150.

higher than the 123.1 mA h g^{-1} of S-LFP. Additionally, R-LFP-150 demonstrated a smaller potential interval compared to S-LFP (Fig. S5, ESI†) and a lower charge transfer resistance (R_{ct}) (Fig. S6, ESI†), highlighting the superior effect of the regeneration process.

The low-rate cycling performance was evaluated at a 0.2C rate (Fig. 4(b)). R-LFP-150 exhibited an initial capacity of 159.2 mA h g^{-1} and maintained stable performance over 200 cycles, retaining 147.5 mA h g^{-1} at the end. R-LFP-120 showed an initial capacity of 138.8 mA h g^{-1}, stabilizing at 130.4 mA h g^{-1} after 200 cycles. Both R-LFP-150 and R-LFP-120 demonstrated significant capacity improvements compared to the S-LFP electrode, which delivered 116.8 mA h g^{-1} in the first cycle and 103.5 mA h g^{-1} after 200 cycles. The slightly lower capacity of R-LFP-120 compared to R-LFP-150 is attributed to the residual impurity phase of $FePO_4$ (as shown in Fig. 2(a)), which does not contribute to capacity.[27] In contrast, the R-LFP-180 electrode exhibited an initial capacity of 113.1 mA h g^{-1}, lower than that of S-LFP, which might be due to the formation of the new $Fe_5(PO_4)_4(OH)_3{\cdot}2H_2O$ phase (Fig. 2(c)).

Fig. 4(c) and Fig. S7 (ESI†) illustrate the rate performance of R-LFP and S-LFP at various current rates (0.1, 0.2, 0.5, and 1C). The reversible specific capacities of R-LFP-150 were 163.1,

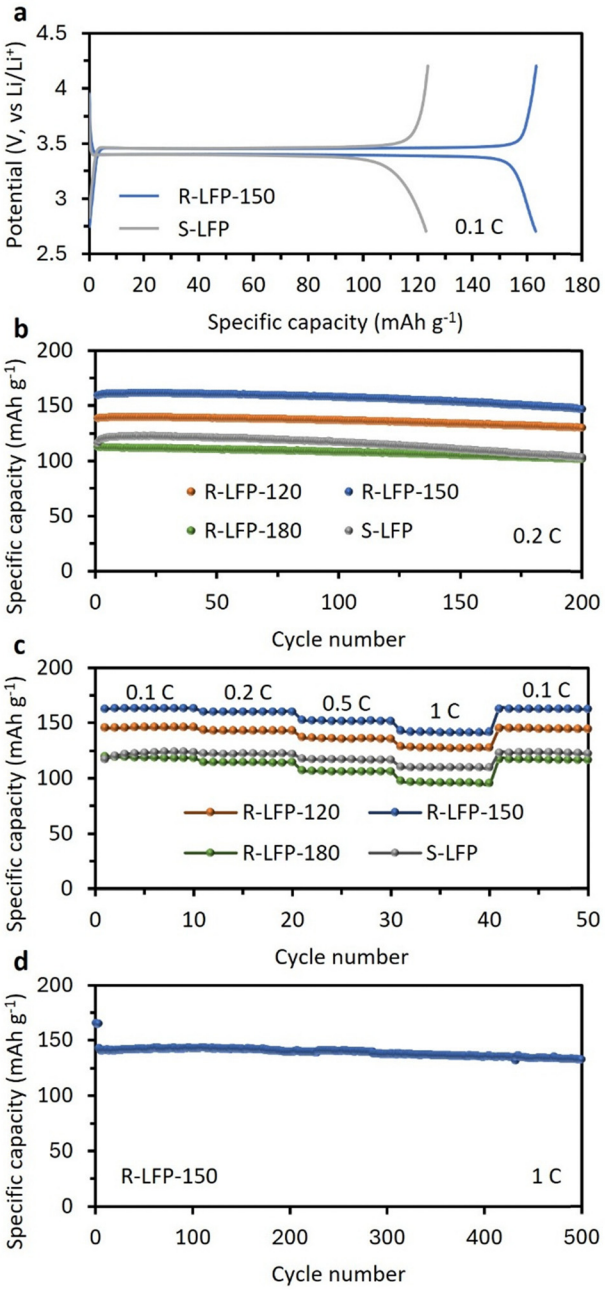

Fig. 4 (a) 0.1C Charge and discharge curves of R-LFP-150 and S-LFP. (b) 0.2C cycling performance and (c) rate performance comparation of R-LFP-120, R-LFP-150, R-LFP-180 and S-LFP. (d) long cycling performance of R-LFP-150.

160.2, 151.6, and 141.7 mA h g^{-1}, respectively. Upon returning to a 0.1C rate, a capacity of 162.5 mA h g^{-1} was recovered, demonstrating superior rate performance compared to S-LFP, which exhibited specific capacities of 123.1, 122.2, 117.2, and 109.7 mA h g^{-1}. Similarly, R-LFP-120 showed enhanced performance over S-LFP, delivering capacities of 146.0, 143.1, 135.9, and 127.5 mA h g^{-1}. However, for R-LFP-180, the low-rate capacity was comparable to that of S-LFP, but at higher charging/discharging rates, the capacity declined more significantly, indicating that excessively high regeneration temperatures

adversely affect lithium replenishment and induce new phase generation, as demonstrated by the XRD pattern in Fig. 2(c).

We further investigated the high-rate (1C) cycling performance of R-LFP-150 (Fig. 4(d)). The electrode delivered 142.9 mA h g^{-1} in the first 1C discharge. After 500 cycles, it retained a capacity of 133.2 mA h g^{-1}, with an exceptionally low degradation rate of 0.013%.

In summary, this study demonstrates the effectiveness of oxalic acid and lithium hydroxide as both reducing agents and lithium sources for the efficient regeneration of spent $LiFePO_4$ materials. The effects of reaction temperature, reagent dosage, structural composition, and electrochemical performance were systematically investigated and optimized. The regenerated $LiFePO_4$ (R-LFP-150) exhibited enhanced electrochemical performance, delivering an initial capacity of 159.2 mA h g^{-1} at 0.2C and maintaining stability over 200 cycles. This method provides a viable approach for directly regenerating spent $LiFePO_4$ from various degradation states, significantly enhancing its feasibility for practical applications.

J. Z. Q. W. and Z. L. conceived the original concept and initiated the project. J. Z. mainly performed the cycling of cylindrical cells, chemical treatment, SEM, XRD, and electrochemical performance. S. Z. and N. T. helped partial experiments. H. T. carried out TEM and EELS test. W. W. carried out XPS test. J. Z. wrote the manuscript.

Data availability

All the data supporting this article have been included in the main text and the ESI.†

This work was financially supported by a grant for Programmatic Funds (MTC Domain, grant no. M24N5b0037, project reference no. SC25/24-843926) from the Agency for Science, Technology and Research (A*STAR), Singapore.

Conflicts of interest

There are no conflicts to declare.

Notes and references

1 Y. Hua, X. Liu, S. Zhou, Y. Huang, H. Ling and S. Yang, *Resour., Conserv. Recycl.*, 2021, **168**, 105249.
2 Z. Yang, H. Huang and F. Lin, *Adv. Energy Mater.*, 2022, **12**, 2200383.
3 C. Y. Yang, Z. Jiang, X. Y. Chen, W. Luo, T. F. Zhou and J. P. Yang, *Chem. Commun.*, 2024, **60**, 10245.
4 D. Kamath, R. Arsenault, H. C. Kim and A. Anctil, *Environ. Sci. Technol.*, 2020, **54**, 6878.
5 R. Ma, S. Tao, X. Sun, Y. Ren, C. Sun, G. Ji, J. Xu, X. Wang, X. Zhang, Q. Wu and G. Zhou, *Nat. Commun.*, 2024, **15**, 7641.
6 A. Nurdiawati and T. K. Agrawal, *Resour., Conserv. Recycl.*, 2022, **185**, 106484.
7 M. Y. Chen, X. T. Ma, B. Chen, R. Arsenault, P. Karlson, N. Simon and Y. Wang, *Joule*, 2019, **3**, 2622.
8 G. Harper, R. Sommerville, E. Kendrick, L. Driscoll, P. Slater, R. Stolkin, A. Walton, P. Christensen, O. Heidrich, S. Lambert, A. Abbott, K. S. Ryder, L. Gaines and P. Anderson, *Nature*, 2019, **575**, 75.
9 J. Z. Yu, X. Wang, M. Y. Zhou and Q. Wang, *Energy Environ. Sci.*, 2019, **12**, 2672.
10 J. T. Hu, J. L. Zhang, H. X. Li, Y. Q. Chen and C. Y. Wang, *J. Power Sources*, 2017, **351**, 192.
11 Z. Xing and M. Srinivasan, *Chem. Eng. J.*, 2023, **474**, 145306.
12 H. Y. Wang, K. Huang, Y. Zhang, X. Chen, W. Jin, S. L. Zheng, Y. Zhang and P. Li, *ACS Sustainable Chem. Eng.*, 2017, **5**, 11489.
13 P. P. Xu, D. H. S. Tan, B. L. Jiao, H. P. Gao, X. L. Yu and Z. Chen, *Adv. Funct. Mater.*, 2023, **33**, 2213168.
14 G. H. Jiang, Y. N. Zhang, Q. Meng, Y. J. Zhang, P. Dong, M. Y. Zhang and X. Yang, *ACS Sustainable Chem. Eng.*, 2020, **8**, 18138.
15 R. Shi, N. Zheng, H. Ji, M. Zhang, X. Xiao, J. Ma, W. Chen, J. Wang, H. M. Cheng and G. Zhou, *Adv. Mater.*, 2024, **36**, e2311553.
16 B. B. Chen, M. Liu, S. Cao, H. Hu, G. R. Chen, X. W. Guo and X. Y. Wang, *J. Alloys Compd.*, 2022, **924**, 166487.
17 S. P. Hao, Y. L. Lv, Y. Zhang, S. W. Liu, Z. L. Tan, W. Liu, Y. G. Xia, W. Yin, Y. Q. Liao, H. J. Ji, Y. L. Kong, Y. D. Shao, Y. H. Huang and L. X. Yuan, *Energy Environ. Sci.*, 2025, **18**, 3750.
18 J. Tang, H. T. Qu, C. B. Sun, X. Xiao, H. C. Ji, J. X. Wang, J. F. Li, G. J. Ji, X. Zhang, H. M. Cheng and G. M. Zhou, *Adv. Mater.*, 2025, **37**, 2420238.
19 K. Jia, G. Yang, Y. He, Z. Cao, J. Gao, H. Zhao, Z. Piao, J. Wang, A. M. Abdelkader, Z. Liang, R. V. Kumar, G. Zhou, S. Ding and K. Xi, *Adv. Mater.*, 2024, **36**, e2313273.
20 Y. Cao, J. Li, D. Tang, F. Zhou, M. Yuan, Y. Zhu, C. Feng, R. Shi, X. Wei, B. Wang, Y. Song, H. M. Cheng and G. Zhou, *Adv. Mater.*, 2024, **36**, e2414048.
21 Z. T. Fei, Y. Y. Su, Y. C. Zha, X. H. Zhao, Q. Meng, P. Dong and Y. J. Zhang, *Chem. Eng. J.*, 2023, **464**, 142534.
22 B. Zhang, Y. Xu, B. Makuza, F. Zhu, H. Wang, N. Hong, Z. Long, W. Deng, G. Zou, H. Hou and X. Ji, *Chem. Eng. J.*, 2023, **452**, 139258.
23 J. F. Xiao, J. Li and Z. M. Xu, *Environ. Sci. Technol.*, 2017, **51**, 11960.
24 X. Chang, M. Fan, C. F. Gu, W. H. He, Q. H. Meng, L. J. Wan and Y. G. Guo, *Angew. Chem., Int. Ed.*, 2022, **61**, e202202558.
25 L. Li, Y. F. Bian, X. X. Zhang, Y. B. Guan, E. S. Fan, F. Wu and R. J. Chen, *Waste Manage.*, 2018, **71**, 362.
26 T. Yingnakorn, J. Hartley, J. S. Terreblanche, C. H. Lei, W. M. Dose and A. P. Abbott, *RSC Sustainability*, 2023, **1**, 2341.
27 P. P. Xu, Q. Dai, H. P. Gao, H. D. Liu, M. H. Zhang, M. Q. Li, Y. Chen, K. An, Y. S. Meng, P. Liu, Y. R. Li, J. S. Spangenberger, L. Gaines, J. Lu and Z. Chen, *Joule*, 2020, **4**, 2609.
28 Z. Y. Jiang, J. Sun, P. S. Jia, W. L. Wang, Z. L. Song, X. Q. Zhao and Y. P. Mao, *Sustainable Energy Fuels*, 2022, **6**, 2207.
29 T. Ouaneche, L. Stievano, F. Rabuel, A. Jamali, C. Guery, L. Monconduit, M. T. Sougrati and N. Recham, *Batteries Supercaps*, 2025, e202400765.
30 D. Tang, G. J. Ji, J. X. Wang, Z. Liang, W. Chen, H. C. Ji, J. Ma, S. Liu, Z. F. Zhuang and G. M. Zhou, *Adv. Mater.*, 2024, **36**, e2309722.

